SPECTRAL L^2-DISTANCE FOR INTRINSIC 3D SHAPE ANALYSIS

RONGJIE LAI*, YONGGANG SHI†, AND TONY F. CHAN‡

Abstract. One of the main challenges in 3D shape analysis is the comparison of surfaces according to rigorous metrics that can capture their intrinsic differences. A well-defined metric should be invariant to translation, rotation, scaling, articulation, and more generally, isometric variations. On the other hand, surfaces are typically represented as embedding manifolds in 3D where the explicit use of Euclidean coordinates makes it difficult to achieve the above invariance. To overcome this difficulty, we propose in this work a novel metric, the spectral l^2-distance, based on optimizing the surface Laplace-Beltrami spectral embedding. Because the Laplace-Beltrami eigen-system is isometry invariant, the proposed distance automatically satisfies the desired invariance. We also prove that the spectral l^2-distance meets the conditions of a metric, which allows the rigorous comparison of intrinsic shape differences. One key advantage of this novel metric is that it enables us to perform robust analysis of global shape differences and local shape features. For global shape analysis, we apply it to surface classification and show that it can achieve intuitively meaningful results. For local shape analysis, we develop a template matching approach in the optimal embedding space to tackle the challenging problem of identifying major sulci on vervet cortices. To further demonstrate its power in local analysis, we design a direct surface mapping algorithm based on the correspondence induced from the spectral l^2-distance and illustrate its application on mapping cortical surfaces.

Key words. Laplace-Beltrami eigen-system, Spectral l^2-distance, Surface Classification, Local Pattern Identification, Surface Mapping.

AMS subject classifications. 15A15, 15A09, 15A23

1. Introduction.

Research in 3D surface analysis, which studies topics such as classification, mapping, local and global pattern analysis, has important applications in many fields including computer vision, computer graphics, and medical image analysis [16, 20, 58, 22]. Among various 3D shape analysis tasks, surface comparison is a fundamental problem, which ideally should quantitatively measure global shape differences and provide guidance to pinpoint these differences locally. On the other hand, surfaces are typically represented as embedding manifolds in $\mathbb{R}^3$, where it is well known that intrinsically identical surfaces can have significantly different representations due to actions such as translation, rotation, and more general isometric transformations. To overcome this difficulty, one key challenge is to construct a rigorous metric that measures *intrinsic* differences among surfaces. Motivated by the global embedding framework with Laplace-Beltrami eigen-system proposed by P. Bérard et al. [3], we develop in this paper a novel metric, the spectral l^2-distance, based on optimizing the Laplace-Beltrami spectral embedding of surfaces. This distance provides a new way of measuring surface differences and performing detailed shape analysis.

There are generally three different classes of approaches to compare surfaces using intrinsic geometry. In early works, feature-based methods were developed in computer vision and graphics to compare surfaces in an intrinsic fashion. Various features were proposed such as shape contexts, shape distributions, shape inner distance, conformal factor, [43, 1, 18, 34, 57, 2] to characterize different aspects of surface geometry. Because such features are usually application driven, they lack generality and does not typically have mathematically rigorous distance measures. The shape-space approach overcomes this difficulty by introducing metric structures on the space of all surfaces, where the distance between two surfaces can be measured by the metric structure introduced for the shape space. For instance, the Teichm$\ddot{u}$ller space, geodesic spectra and the computation of Teichm$\ddot{u}$ller coordinates is discussed in [36, 24, 25]. However, the extraction of local differences are difficult

*Department of Mathematics, University of Southern California, Los Angeles, CA, USA (rongjiel@usc.edu)

†Lab. of Neuro Imaging, University of California, Los Angeles, CA, USA (yshi@loni.ucla.edu)

‡Department of Mathematics and Department of Computer Science and Engineering, Hong Kong University of Science and Technology, HongKong (tonyfchan@ust.hk)

because each surface is viewed as a point in the shape space. More recently, a third class of approaches were introduced based on the metric geometry [11]. In this approach, each surface is treated as a metric space and surfaces are compared according to the theory of metric geometry by measuring their Gromov-Hausdorff distance and Gromov-Wasserstein distance [41, 38, 39, 40]. Diffusion distance [29, 15] on surface was applied to compute the Gromov-Hausdorff distance and compare non-rigid geometry based on the metric geometry [9]. While theoretically this class of methods can compute both local and global surface differences, the need for optimization over all possible correspondences makes it computationally challenging to conduct detailed analysis of surface structures.

More recently, there have been increasing interests in using the Laplace-Beltrami (LB) eigen-system in 3D surface analysis because it depends only on intrinsic geometry, is general for arbitrary shapes, and easy to compute. Using LB eigenvalues as "shape DNA" [47], a shape classification method was first proposed. However, the LB eigenvalues are not enough to completely determine surface geometry [28, 42, 56, 44, 21, 31]. By combining LB eigenvalues and eigenfunctions, a series of interesting works have been developed for surface characterization and applied to surface mesh processing [33, 60], surface quadrangulation [17], skeleton construction [51], Hierarchical shape segmentation [46], 3D surface reconstruction [52], surface local parametrization [26], and heat kernel signatures (HKS) [55, 10].

For surface comparison, the LB eigen-system has been used to construct a common embedding space to measure shape differences. A global embedding framework was proposed by P. Bérard et al. [3] that uses heat kernel of the LB operator. In this framework, the distance of surfaces is defined as the Gromov-Hausdorff distance of their embeddings. However, this distance depends on the selection of the diffusion time and is not scale invariant. In practice, the Gromov-Hausdorff distance could be sensitive to noise and it is interesting to develop more robust distance measures in the embedding space. Instead of using heat kernel, Rustamov [48] introduced an embedding called the Global Position Signature (GPS), which is related to the Green function of the LB operator. This embedding is scale invariant, but is non-unique because of the sign-ambiguity and multiplicity in the eigen-system. To overcome this limitation, a heuristic histogram feature was introduced to measure surface differences.

Motivated by the global embedding framework in [3] and the GPS embedding in [48], this work proposes a novel and mathematically well-defined metric, spectral l^2-distance. This distance is defined over all possible GPS embeddings, which takes into account the ambiguity in the LB eigen-system, and we prove it is a rigorous metric. Compared with Gromov-Hausdorff distance, the spectral l^2-distance integrates over the whole surface and is thus more robust to noise. Because the GPS embedding is isometry and scale invariant, the proposed spectral l^2-distance also has this property. In particular, it is invariant to translation, rotation, scaling and more general pose variations such as articulation. The mathematical rigorousness of the proposed spectral l^2-distance provides us a solid foundation to study surface comparisons. Moreover, the optimal embedding bases induced from the spectral l^2-distance can be powerful tools to perform both global and local surface comparisons. To demonstrate the application of the spectral l^2-distance and the corresponding optimal embedding bases, we develop practical algorithms to solve various shape analysis problems. We first applied the proposed distance to perform 3D non-rigid surface classification and promising results are presented. Using the optimal embedding bases, we developed a novel algorithm to solve the challenging sulci identification problem in brain imaging. Furthermore, the potential of the optimal embedding bases in surface mapping is demonstrated by showing its performance on mapping the white and gray matter boundaries of the cortex.

2. Mathematical Background. In this section, we first review the concept of the Laplace-Beltrami (LB) eigen-system on general surfaces and the numerical scheme for its computa-

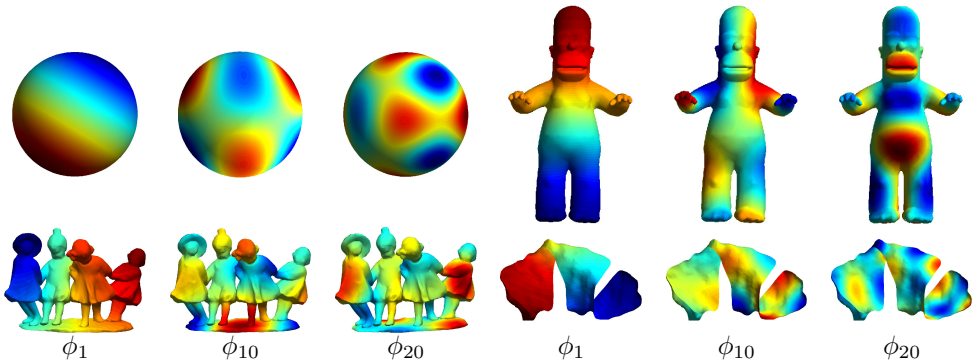

FIG. 2.1. *Laplace-Beltrami Eigenfunctions obtained by the finite element method are color coded on surfaces.*

tion on triangular meshes using the finite element method. The spectral l^2-distance is then proposed as an intrinsic metric to compare surfaces. Proofs will be provided that show the proposed distance satisfying the conditions of rigorous metric.

2.1. The Laplace-Beltrami Eigen-system. Let $(\mathcal{M}, g)$ be a closed Riemannian surface. For any smooth function $\phi \in C^\infty(\mathcal{M})$, the LB operator in a local coordinate system $\{(x^1, x^2)\}$ is defined as the following coordinate invariant form [27]:

$$\triangle_{\mathcal{M}}\phi = \frac{1}{\sqrt{G}}\sum_{i=1}^{2}\frac{\partial}{\partial x_i}(\sqrt{G}\sum_{j=1}^{2} g^{ij}\frac{\partial \phi}{\partial x_j}) \tag{2.1}$$

where (g^{ij}) is the inverse matrix of $g = (g_{ij})$ and $G = \det(g_{ij})$.

The LB operator is self-adjoint and elliptic, so its spectrum is discrete. We denote the eigenvalues of $\triangle_{\mathcal{M}}$ as $0 = \lambda_0 < \lambda_1 < \lambda_2 < \cdots$ and the corresponding eigenfunctions as $\phi_0, \phi_1, \phi_2, \cdots$ such that

$$\triangle_{\mathcal{M}}\phi_k = -\lambda_k\phi_k, \quad k = 0, 1, 2, \cdots. \tag{2.2}$$

If $(\mathcal{M}, g)$ is an open Riemannian surface with boundary $\partial\mathcal{M}$ and $\vec{n}$ is the unit normal vector filed of $\partial\mathcal{M}$ with respect to $\mathcal{M}$, we consider the LB eigen-system with Nuemann boundary condition:

$$\begin{aligned} \triangle_{\mathcal{M}}\phi_k &= -\lambda_k\phi_k, \\ \nabla_{\mathcal{M}}\phi \cdot \vec{n}|_{\partial\mathcal{M}} &= 0, \qquad k = 0, 1, 2, \cdots. \end{aligned} \tag{2.3}$$

The set of eigenfunctions $\{\phi_n\}$ forms an orthonormal basis of the space of smooth functions on $\mathcal{M}$. The set $\{\lambda_n, \phi_n\}$ is called the LB eigen-system of $(\mathcal{M}, g)$. Let $E_i = \{u \in C^2(\mathcal{M}) \mid \triangle_{\mathcal{M}}u = -\lambda_i u\}$ denote the eigenspace associated with the eigenvalue λ_i. If the eigenspace of all eigenvalues are one dimensional, the eigen-system $\{\lambda_i, \phi_i\}_{i=0}^{\infty}$ of $\mathcal{M}$ is called *simple* [14].

To numerically solve (2.2) and (2.3), we consider the following weak formula of these two equations:

$$\int_{\mathcal{M}} \nabla_{\mathcal{M}}\phi_k \nabla_{\mathcal{M}}\eta = \lambda \int_{\mathcal{M}} \phi_k\eta, \qquad \forall\, \eta \in C^\infty(\mathcal{M}) \tag{2.4}$$

By using the finite element method (FEM), we can solve this weak formula numerically and compute the eigen-system of the LB operator [47]. Given a surface $\mathcal{M}$ in $\mathbb{R}^3$, we represent

$\mathcal{M}$ as a triangular mesh $\{V = \{v_i\}_{i=1}^N, T = \{T_l\}_{l=1}^L\}$, where $v_i \in \mathbb{R}^3$ is the i-th vertex and T_l is the l-th triangle. One can choose linear elements $\{e_i\}_{i=1}^N$ satisfying $e_i(v_j) = \delta_{i,j}$ as the notation of Kronecker delta symbol, and write $S = Span_{\mathbb{R}}\{e_i\}_{i=1}^N$. Then the discrete version of the weak formula (2.4) is to find a $\phi \in S$, such that

$$\sum_l \int_{T_l} \nabla_{\mathcal{M}} \phi \nabla_{\mathcal{M}} \eta = \lambda \sum_l \int_{T_l} \phi\eta, \quad \forall \eta \in S. \tag{2.5}$$

If we write

$$\begin{cases} \phi = \sum_i^N x_i e_i \\ A = (a_{ij})_{N\times N}, a_{ij} = \sum_l \int_{T_l} \nabla_{\mathcal{M}} e_i \nabla_{\mathcal{M}} e_j \\ B = (b_{ij})_{N\times N}, b_{ij} = \sum_l \int_{T_l} e_i e_j, \end{cases} \tag{2.6}$$

where the stiffness matrix A is symmetric and the mass matrix B is symmetric and positive definite, we can compute the LB eigen-system by solving the generalized matrix eigenproblem:

$$\begin{cases} Ax = \lambda Bx, \text{where } x = (x_1, \cdots, x_N)^T \\ \phi = \sum_i^N x_i e_i \end{cases} \tag{2.7}$$

Note that both A and B are sparse matrices of size $N \times N$. There are a variety of numerical packages, such as MATLAB, to solve the above problem. In Figure 2.1, we illustrate our computational results for LB eigenfunctions on different types of surfaces. It demonstrates that the LB eigen-systems of different types of surfaces, such as the standard sphere, surfaces with complicated geometry, surfaces with high genus, and open surfaces, can be robustly computed with the finite element method.

From the signal processing point of view, the eigenfunctions of the LB operator are natural extensions of the Fourier basis functions from the Euclidean domain to general manifolds. Another famous example is the spherical harmonics, which are the eigenfunctions of the LB operator on the unit sphere, and they have been used in various functional analysis tasks on spheres. Similar to Fourier analysis in Euclidean space and harmonic analysis on spheres, the LB eigen-systems are also powerful tools for function analysis on surfaces. In particular, we would like to list the following two remarkable properties of the LB eigensystem [49, 23].

- Due to the intrinsic properties of LB operator $\triangle_{\mathcal{M}}$, the induced LB eigen-systems $\{\lambda_i, \phi_i\}_{i=0}^{\infty}$ are also completely intrinsic geometric quantities. In particularly, surface LB eigen-systems are robust to translation, rotation and pose variations.
- Scale formula: Let c be a positive constant, $\{\lambda_i, \phi_i\}$ be the eigensystem of $(\mathcal{M}, g)$, and $\{\tilde{\lambda}_i, \tilde{\phi}_i\}$ be the eigensystem of $(\mathcal{M}, c \cdot g)$, then

$$\lambda_i = c \cdot \tilde{\lambda}_i \text{ and } \phi_i = \sqrt{c} \cdot \tilde{\phi}_i \tag{2.8}$$

In Figure 2.2, we demonstrate the intrinsic properties of LB eigenfunctions on five different poses of the shape David obtained from nonrigid shape database TOSCA [5, 7, 8]. Five different poses of David are color coded by LB eigenfunctions with their zero level contours marked in red color. It is easy to see the pose invariance of LB eigenfunctions and the corresponding zero level contours across the group of the shape David with different poses.

More importantly, the LB eigen-systems are not only useful for functional analysis on surfaces but also powerful for studying the intrinsic geometry of the underlying surfaces. One of the most famous examples to study surface geometry using LB eigen-systems is Kac's question [28]: "Can one hear a shape of a drum?" Namely, can we determine the geometry of

FIG. 2.2. *The first row: The surfaces are color coded by the corresponding first LB eigenfunctions and the red contours mark the zero level line of the first LB eigenfunctions. The second row: The surfaces are color coded by the corresponding fifth LB eigenfunctions and the red contours mark the zero level line of the fifth LB eigenfunctions.*

surfaces using their LB eigenvalues? The relation between geometry of surfaces and their LB eigenvalues was illustrated by heat trace formula [37]. However, LB eigenvalues, which are just a part of LB eigen-systems, can not completely determine surface geometry [42, 56, 44, 21]. More fruitful information are stored in LB eigenfunctions. Bérard [3] introduced the first theoretical result about using LB eigen-system as global embedding to analyze manifolds. More recently, there have been increasing interests in using LB eigen-systems to study 3D surface analysis problems. M. Reuter [47] proposed to use LB eigenvalues as fingerprints to classify surfaces. Rustamov[48] was one of the first to use global embedding obtained by LB eigen-system to analyze surfaces. P. Jones et al. [26] introduced a new manifold local parametrization approach using LB eigenfunctions. J. Sun, M. Bronstein et al. [55, 10] introduced intrinsic surface descriptors using heat kernels of surface heat equations. Recent work [45, 51, 50, 31, 32] proposed many applications of LB eigen-system in medical image analysis.

2.2. Metric in the embedding space. According to the above discussion of the computability and robustness of surface LB eigen-systems, it is reasonable to consider LB eigen-systems as signatures to characterize surfaces. While there have been many successful applications of LB eigen-systems in practical shape analysis, the challenge, however, is to define a meaningful metric to rigorously measure difference of surfaces based on the LB eigen-systems. To tackle this problem, a distance, spectral l^2-distance, will be introduced in this subsection, which depends only on the intrinsic geometry difference of surfaces. Meanwhile, a co-product, optimal embedding bases, of this distance will be introduced. By combining the spectral l^2-distance and optimal embedding bases, we can conduct global and local analysis in surface comparison.

To rigorously discuss the the underline definition space of the spectral l^2 distance, we would like to first introduce the **scale invariant shape space** formalized as follows.

DEFINITION 2.1 (shape scale equivalence). *Given two surfaces $(\mathcal{M}, g)$ and $(\tilde{\mathcal{M}}, \tilde{g})$. Let f be a diffeomorphism from $\mathcal{M}$ to $\tilde{\mathcal{M}}$. Then f can naturally induce a pull-back metric on $\mathcal{M}$ as follows [27]:*

$$(f^*\tilde{g})(v_1, v_2) = \tilde{g}(f_*(v_1), f_*(v_2)) \tag{2.9}$$

where v_1, v_2 are any two tangent vector fields on $\mathcal{M}$. We call $(\mathcal{M}, g)$ is equivalent to $(\tilde{\mathcal{M}}, \tilde{g})$

if and only if there is a diffeomorphism $f : \mathcal{M} \to \tilde{\mathcal{M}}$ *and a constant* c *such that* $g = c \cdot f^*(\tilde{g})$*, which is denoted by* $(\mathcal{M}, g) \sim (\tilde{\mathcal{M}}, \tilde{g})$.

This equivalence relation characterize the intrinsic shape difference. In other words, we view two surfaces to be the same if and only if they are isometric to each other up to a constant scaling factor. With the above equivalence relation, we can define **scale invariant shape space** as follows.

DEFINITION 2.2 (scale invariant shape space). *Let* $\mathfrak{W}$ *be the set of all surfaces. The scale invariant shape space* $\mathfrak{D}$ *is defined by the set of the equivalent classes describe by the above equivalence relation. i.e.* $\mathfrak{D} = \{(\mathcal{M}, g)\}/\sim$.

Obiviously, the quotient space $\mathfrak{D}$ is equivalent to the set of all surfaces with normalized area, namely $\mathfrak{D} \cong \mathfrak{S} = \{(\mathcal{M}, g) \mid \text{Area}(\mathcal{M}) = 1\}/\sim$. Remember our goal is to perform translation, rotation, scale and pose invariant surface analysis. More precisely speaking, we need to analyze objects in the scale invariant shape space $\mathfrak{D}$ in which only surface intrinsic geometry is described. To conduct surface analysis in the shape space $\mathfrak{D}$, one of the most essential tools is to endure a well-behaved metric on $\mathfrak{D}$, then many other work, such as surface classification, surface comparison etc. can be followed. To achieve this goal, we will introduce the spectral l^2-distance using LB eigen-system discussed in section 2.1.

Given a surface $(\mathcal{M}, g)$ and its LB eigen-system $\Phi = \{\lambda_i, \phi_i\}$, the scale-invariant embedding proposed in [48] is defined as:

$$I^{\Phi}_{\mathcal{M}}(x) = \{\frac{\phi_1(x)}{\sqrt{\lambda_1}}, \frac{\phi_2(x)}{\sqrt{\lambda_2}}, \cdots, \frac{\phi_k(x)}{\sqrt{\lambda_k}}, \cdots\}, \quad \forall x \in \mathcal{M} \tag{2.10}$$

In Fig. 2.3, we show the embedding results of the unit sphere and a cortical surface using the first three eigenfunctions. Generally speaking, the more eigenfunctions we use, the more detailed information of the surface we can obtain.

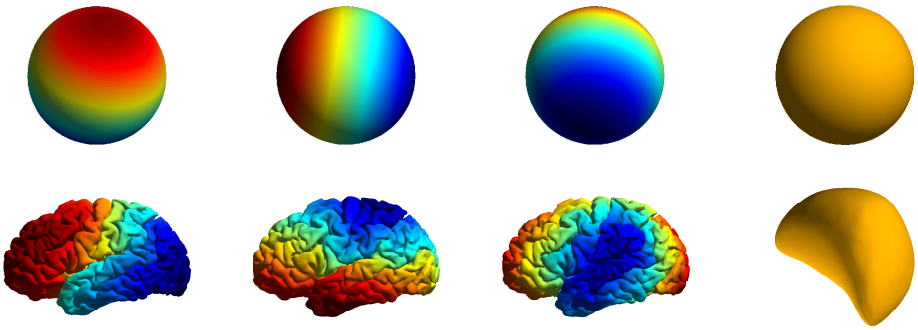

FIG. 2.3. *The first three columns are color coded by the first three eigenfunctions on each surface respectively. The last column is obtained using the first three eigenfunctions as 3 coordinates to reconstruct the original surfaces*

Due to the separable properties of LB eigen-system, the following theorem is demonstrated in [48], which shows that the map in (2.10) is an embedding.

THEOREM 2.3. *For any given surface* $(\mathcal{M}, g)$*, any given basis* $\Phi = \{\phi_i\}$*, the map* $I^{\Phi}_{\mathcal{M}}$ *is an embedding and it is scale invariant by the scale formula (2.8).*

The biggest advantage of this embedding is that we can put all surfaces into a common space to factor out all pose and scale variations. However, the main challenge in constructing a well-defined distance in the embedding space is that the eigen-system of a given surface $\mathcal{M}$ is not unique. The mapping $I_{\mathcal{M}}$ depends on the choice of an orthonormal basis of eigenfunctions. For instance, both ϕ_i and $-\phi_i$ can be an element of basis. For eigenvalues with multiplicity greater than one, there is even more freedom to choose the basis. To overcome

this difficulty, a modification of G2 distributions was proposed in [48] to describe the "distance" between two surfaces. However, the G2 distribution may not be a rigorous distance. Inspired by P.Bérard et.al's work about heat kernel embedding [3], we propose the **spectral l^2-distance** as a metric to measure surface difference in the embedding space.

Given a surface$(\mathcal{M}, g)$, one can decompose the space $L^2(\mathcal{M}, g)$ as $L^2(\mathcal{M}, g) = \bigoplus_{i=0}^{\infty} E_i$, where E_i's are the eigenspaces of the LB operator $\triangle_{\mathcal{M}}$ associated with eigenvalue λ_i. We denote $\mathcal{B}(\mathcal{M}) = \prod_{i=0}^{\infty} \mathcal{B}(E_i)$ the set of corresponding orthonormal bases. The space $\mathcal{B}(E_i)$ can be identified with the orthogonal group $O(dim(E_i))$ and hence $\mathcal{B}(\mathcal{M})$ is a compact set with respect to the product topology. The **spectral l^2-distance** for any given two surfaces $(\mathcal{M}, g), (\tilde{\mathcal{M}}, \tilde{g})$ is defined as follows.

DEFINITION 2.4 (spectral l^2-distance). *Let $(\mathcal{M}, g)$ and $(\tilde{\mathcal{M}}, \tilde{g})$ be two surfaces. For any given LB orthonormal basis Φ of $\mathcal{M}$ and $\tilde{\Phi}$ of $\tilde{\mathcal{M}}$, we define*

$$\begin{aligned} d_{\Phi}^{\tilde{\Phi}}(x, \tilde{\mathcal{M}}) &= \inf_{y \in \tilde{\mathcal{M}}} ||I_{\mathcal{M}}^{\Phi}(x) - I_{\tilde{\mathcal{M}}}^{\tilde{\Phi}}(y)||_2 \ , \ \forall \ x \in \mathcal{M} \\ d_{\Phi}^{\tilde{\Phi}}(\mathcal{M}, y) &= \inf_{x \in \mathcal{M}} ||I_{\mathcal{M}}^{\Phi}(x) - I_{\tilde{\mathcal{M}}}^{\tilde{\Phi}}(y)||_2 \ , \ \forall \ y \in \tilde{\mathcal{M}}. \end{aligned} \tag{2.11}$$

The spectral pre-l^2-distance between $\mathcal{M}$ and $\tilde{\mathcal{M}}$ with respect to $\Phi, \tilde{\Phi}$ is defined by:

$$d_{\Phi}^{\tilde{\Phi}}(\mathcal{M}, \tilde{\mathcal{M}}) = \max \Big\{ \int_{\mathcal{M}} d_{\Phi}^{\tilde{\Phi}}(x, \tilde{\mathcal{M}}) \mathrm{d}_{\mathcal{M}}(x) \ , \int_{\tilde{\mathcal{M}}} d_{\Phi}^{\tilde{\Phi}}(\mathcal{M}, y) \mathrm{d}_{\tilde{\mathcal{M}}}(y) \Big\} \tag{2.12}$$

where $\mathrm{d}_{\mathcal{M}}(x), \mathrm{d}_{\tilde{\mathcal{M}}}(y)$ are normalized area elements, i.e., $\int_{\mathcal{M}} \mathrm{d}_{\mathcal{M}}(x) = 1$ and $\int_{\tilde{\mathcal{M}}} \mathrm{d}_{\tilde{\mathcal{M}}}(y) = 1$. The spectral l^2-distance $d(\mathcal{M}, \tilde{\mathcal{M}})$ between $\mathcal{M}$ and $\tilde{\mathcal{M}}$ independent of the choice of eigen-systems is then defined as:

$$d(\mathcal{M}, \tilde{\mathcal{M}}) = \inf_{\Phi \in \mathcal{B}(\mathcal{M}), \tilde{\Phi} \in \mathcal{B}(\tilde{\mathcal{M}})} \max \Big\{ \int_{\mathcal{M}} d_{\Phi}^{\tilde{\Phi}}(x, \tilde{\mathcal{M}}) \mathrm{d}_{\mathcal{M}}(x) \ , \int_{\tilde{\mathcal{M}}} d_{\Phi}^{\tilde{\Phi}}(\mathcal{M}, y) \mathrm{d}_{\tilde{\mathcal{M}}}(y) \Big\}. \tag{2.13}$$

Because $\mathcal{B}(\mathcal{M})$ and $\mathcal{B}(\tilde{\mathcal{M}})$ are compact, $d(\mathcal{M}, \tilde{\mathcal{M}})$ can attain the optimal value for certain $\Phi^* \in \mathcal{B}(\mathcal{M}), \tilde{\Phi}^* \in \mathcal{B}(\tilde{\mathcal{M}})$, which are called the **optimal embedding bases** of the pair $\{\mathcal{M}, \tilde{\mathcal{M}}\}$. The corresponding embedding $I_{\mathcal{M}}^{\Phi^*}$ and $I_{\tilde{\mathcal{M}}}^{\tilde{\Phi}^*}$ are called the **optimal embedding pair** of $\{\mathcal{M}, \tilde{\mathcal{M}}\}$.

Note that surface LB eigen-systems satisfy the robustness property as discussed in Section 2.1. Therefore, the spectral l^2-distance induced from LB eigen-systems also completely reflect the intrinsic geometric difference between two surfaces, which is naturally robust to rotation, translation, scale and pose variations. More precisely, the spectral l^2-distance defined as the above gives a good metic on the scale invariant shape space $\mathfrak{D}$, which is stated in the following theorem:

THEOREM 2.5. *The spectral l^2-distance $d(\cdot, \cdot)$ is a metric on $\mathfrak{S}$. Hence it is also a metric on $\mathfrak{D}$.*

With this theorem, the spectral l^2-distance can provide a rigorous measurement compare surfaces intrinsically and globally. Moreover, one of the big distinction of the spectral l^2-distance is the induced optimal embedding bases, which will provide us a powerful tool to conduct surface feature comparison locally.

For the self-completeness of this paper, we discuss the proof of theorem 2.5 in the rest of this section. This proof is basically split as two lemmas, which can be also found in the conference version of this paper [32]. It is easy to check that $d(\cdot, \cdot)$ is symmetric. To ensure $d(\cdot, \cdot)$ is a metric on $\mathfrak{D}$, we also need the following two lemmas.

LEMMA 2.6 (triangle inequality). *Given any three surfaces* $(\mathcal{M}, g), (\tilde{\mathcal{M}}, \tilde{g}), (\mathcal{N}, \hat{g}) \in \mathfrak{S}$*, then*

$$d(\mathcal{M}, \tilde{\mathcal{M}}) \leq d(\mathcal{M}, \mathcal{N}) + d(\mathcal{N}, \tilde{\mathcal{M}}). \tag{2.14}$$

[Proof]: Given an arbitrary eigen-system Φ of $\mathcal{M}$, $\tilde{\Phi}$ of $\tilde{\mathcal{M}}$, and Θ of $\mathcal{N}$. For any point $x \in \mathcal{M}, y \in \tilde{\mathcal{M}}$ and $z \in \mathcal{N}$. We have:

$$\begin{aligned}
& d_{\Phi}^{\tilde{\Phi}}(x, y) && \leq d_{\Phi}^{\Theta}(x, z) + d_{\Theta}^{\tilde{\Phi}}(z, y) \\
\overset{\inf_{y\in\tilde{\mathcal{M}}}}{\Longrightarrow} \quad & d_{\Phi}^{\tilde{\Phi}}(x, \tilde{\mathcal{M}}) && \leq d_{\Phi}^{\Theta}(x, z) + d_{\Theta}^{\tilde{\Phi}}(z, \tilde{\mathcal{M}}) \\
\overset{\inf_{z\in\mathcal{N}}}{\Longrightarrow} \quad & d_{\Phi}^{\tilde{\Phi}}(x, \tilde{\mathcal{M}}) && \leq d_{\Phi}^{\Theta}(x, \mathcal{N}) + \inf_{z\in\mathcal{N}} d_{\Theta}^{\tilde{\Phi}}(z, \tilde{\mathcal{M}}) \\
& && \leq d_{\Phi}^{\Theta}(x, \mathcal{N}) + d_{\Theta}^{\tilde{\Phi}}(z, \tilde{\mathcal{M}})
\end{aligned}$$

We integrate on $\mathcal{M}$ on the both side of the above inequality.

$$\overset{\int_{\mathcal{M}}}{\Longrightarrow} \quad \int_{\mathcal{M}} d_{\Phi}^{\tilde{\Phi}}(x, \tilde{\mathcal{M}}) \leq \int_{\mathcal{M}} d_{\Phi}^{\Theta}(x, \mathcal{N}) + \int_{\mathcal{M}} d_{\Theta}^{\tilde{\Phi}}(z, \tilde{\mathcal{M}})$$

From the assumption $(\mathcal{M}, g), (\tilde{\mathcal{M}}, \tilde{g}), (\mathcal{N}, \hat{g}) \in \mathfrak{S}$, therefore $\int_{\mathcal{M}} \mathrm{d}_{\mathcal{M}}(x) = \int_{\tilde{\mathcal{M}}} \mathrm{d}_{\tilde{\mathcal{M}}}(x) = \int_{\mathcal{N}} \mathrm{d}vol_{\mathcal{N}}(x) = 1$.

$$\begin{aligned}
\Longrightarrow \quad & \int_{\mathcal{M}} d_{\Phi}^{\tilde{\Phi}}(x, \tilde{\mathcal{M}}) && \leq \int_{\mathcal{M}} d_{\Phi}^{\Theta}(x, \mathcal{N}) + d_{\Theta}^{\tilde{\Phi}}(z, \tilde{\mathcal{M}}) \\
\overset{\int_{\mathcal{N}}}{\Longrightarrow} \quad & \int_{\mathcal{M}} d_{\Phi}^{\tilde{\Phi}}(x, \tilde{\mathcal{M}}) && \leq \int_{\mathcal{M}} d_{\Phi}^{\Theta}(x, \mathcal{N}) + \int_{\mathcal{N}} d_{\Theta}^{\tilde{\Phi}}(z, \tilde{\mathcal{M}})
\end{aligned}$$

Similarly, we can have:

$$\int_{\tilde{\mathcal{M}}} d_{\Phi}^{\tilde{\Phi}}(\mathcal{M}, y) \leq \int_{\mathcal{N}} d_{\Phi}^{\Theta}(\mathcal{M}, z) + \int_{\tilde{\mathcal{M}}} d_{\Theta}^{\tilde{\Phi}}(\mathcal{N}, y).$$

By the definition of $d(\mathcal{M}, \tilde{\mathcal{M}})$ we then have:

$$d(\mathcal{M}, \tilde{\mathcal{M}}) \leq d(\mathcal{M}, \mathcal{N}) + d(\mathcal{N}, \tilde{\mathcal{M}}). \qquad \square$$

LEMMA 2.7 (Positive definiteness). *For any two surfaces* $\mathcal{M}, \tilde{\mathcal{M}}$ *with* $Area(\mathcal{M}) = Area(\tilde{\mathcal{M}})$*,* $d(\mathcal{M}, \tilde{\mathcal{M}}) \geqslant 0$*. Moreover,* $d(\mathcal{M}, \tilde{\mathcal{M}}) = 0$ *if and only if* $\mathcal{M}$ *and* $\tilde{\mathcal{M}}$ *are isometric.*

[Proof]: From the definition of the spectral l^2-distance, it is obviously to have $d(\mathcal{M}, \tilde{\mathcal{M}}) \geqslant 0$. If $\mathcal{M}$ and $\tilde{\mathcal{M}}$ are isometric, we have $d(\mathcal{M}, \tilde{\mathcal{M}}) = 0$ because the LB eigen-system is isometric invariant.

Next we show the opposite is also true. Let $(\mathcal{M}, g), (\tilde{\mathcal{M}}\tilde{g})$ denote two surfaces with the same surface area. By the compactness of $\mathcal{B}(\mathcal{M})$ and $\mathcal{B}(\tilde{\mathcal{M}})$, we can find the optimal eigen-system $\Phi = \{(\lambda_i, \phi_i\}_{i=0}^{\infty}, \tilde{\Phi} = \{(\tilde{\lambda}_i, \tilde{\phi}_i\}_{i=0}^{\infty}$ of $(\mathcal{M}, g), (\tilde{\mathcal{M}}, \tilde{g})$, respectively, such that

$$d(\mathcal{M}, \tilde{\mathcal{M}}) = \max\Big\{ \int_{\mathcal{M}} d_{\Phi}^{\tilde{\Phi}}(x, \tilde{\mathcal{M}}) \, , \int_{\tilde{\mathcal{M}}} d_{\Phi}^{\tilde{\Phi}}(\mathcal{M}, y) \Big\}.$$

Suppose $d(\mathcal{M}, \tilde{\mathcal{M}}) = 0$, we have:

$$d_{\Phi}^{\tilde{\Phi}}(x, \tilde{\mathcal{M}}) = 0, \ \forall \, x \in \mathcal{M} \quad \text{and} \quad d_{\Phi}^{\tilde{\Phi}}(\mathcal{M}, y) = 0, \ \forall \, y \in \tilde{\mathcal{M}}.$$

Therefore,

$$\forall\, x \in \mathcal{M},\ \exists\, y_x = arg\min_{y\in\tilde{\mathcal{M}}} ||I^{\Phi}_{\mathcal{M}}(x) - I^{\tilde{\Phi}}_{\tilde{\mathcal{M}}}(y)||_2 \in \tilde{\mathcal{M}},$$
$$\text{s.t.} \quad \frac{\phi_i(x)}{\sqrt{\lambda_i}} = \frac{\tilde{\phi}_i(y_x)}{\sqrt{\tilde{\lambda}_i}}, \qquad i = 1, 2, \cdots \tag{2.15}$$

We denote $f : \mathcal{M} \to \tilde{\mathcal{M}} : x \longmapsto y_x$, and

$$\forall\, y \in \tilde{\mathcal{M}},\ \exists\, x_y = \arg\min_{x\in\mathcal{M}} ||I^{\Phi}_{\mathcal{M}}(x) - I^{\tilde{\Phi}}_{\tilde{\mathcal{M}}}(y)||_2 \in \mathcal{M},$$
$$\text{s.t.} \quad \frac{\phi_i(x_y)}{\sqrt{\lambda_i}} = \frac{\tilde{\phi}_i(y)}{\sqrt{\tilde{\lambda}_i}}, i = 1, 2, \cdots \tag{2.16}$$

Similarly we define $h : \tilde{\mathcal{M}} \to \mathcal{M} : y \longmapsto x_y$. Both f, h are injective since $I^{\Phi}_{\mathcal{M}}, I^{\tilde{\Phi}}_{\tilde{\mathcal{M}}}$ are one-to-one. Thus $f \circ h = Id_{\tilde{\mathcal{M}}}$ and $h \circ f = Id_{\mathcal{M}}$ and one can easily show that f and h are diffeomorphisms.

Moreover, if we integrate (2.15) for all $i \geq 1$:

$$0 = \int_{\mathcal{M}} \frac{\phi_i(x)}{\sqrt{\lambda_i}} \mathrm{d}_{\mathcal{M}}(x) = \int_{\mathcal{M}} \frac{\tilde{\phi}_i(f(x))}{\sqrt{\tilde{\lambda}_i}} \mathrm{d}_{\mathcal{M}}(x) = \int_{\tilde{\mathcal{M}}} \frac{\tilde{\phi}_i(y)}{\sqrt{\tilde{\lambda}_i}} \mathcal{J}(h) \mathrm{d}_{\tilde{\mathcal{M}}}(y).$$

This means $\mathcal{J}(h)$, which is the Jacobian of h, is orthogonal to all $\tilde{\Phi}_i, i \geq 1$. Therefore, $\mathcal{J}(h)$ must be a constant. On the other hand, we have:

$$\begin{aligned} 1 &= \int_{\mathcal{M}} \mathrm{d}_{\mathcal{M}}(x) = \frac{Area(\tilde{\mathcal{M}})}{Area(M)} \int_{\tilde{\mathcal{M}}} \mathcal{J}(h) \mathrm{d}_{\tilde{\mathcal{M}}}(y) \\ &= \frac{Area(\tilde{\mathcal{M}})}{Area(\mathcal{M})} \mathcal{J}(h) \int_{\tilde{\mathcal{M}}} \mathrm{d}_{\tilde{\mathcal{M}}}(y) = \frac{Area(\tilde{\mathcal{M}})}{Area(\mathcal{M})} \mathcal{J}(h). \end{aligned}$$

So we have $\mathcal{J}(h) = Area(\mathcal{M})/Area(\tilde{\mathcal{M}}) = 1$. Similarly, one can show $\mathcal{J}(f) = 1$.

To conclude, we have shown that both f, h are isometry. Therefore $\mathcal{M}$ is isometric to $\tilde{\mathcal{M}}$. □

In summary, the first lemma proves the triangular inequality of a metric. The second lemma tells us the distance of two surfaces is always nonegative and two surfaces of equal areas are "the same"[1] in R^3 if and only if their spectral l^2-distance is zero. This completes our proof that the spectral l^2-distance is a rigorous metric on $\mathfrak{D}$. Notice that we can construct surface correspondence from formulas (2.15) and (2.16) in the above proof. These two formulas can provide us an algorithm for surface mapping, which will be discussed in Section 6.

3. Numerical Implementation of Spectral l^2-distance. The implementation of the spectral l^2-distance includes two parts, the distance itself and the optimal embedding bases. To implement the spectral l^2-distance in general form is computationally not tractable. However, Uhlenbeck [59] proved that surfaces with simple LB eigen-systems are generic. In other words, most surfaces in practice have simple LB eigen-systems. We describe here how to compute the spectral l^2-distance between surfaces with simple LB eigen-systems.

Let $(\mathcal{M}, g)$ and $(\tilde{\mathcal{M}}, \tilde{g})$ be two surfaces with simple eigen-systems $\Phi = \{(\lambda_i, \phi_i)\}_{i=0}^{\infty}$ and $\tilde{\Phi} = \{(\tilde{\lambda}_i, \tilde{\phi}_i)\}_{i=0}^{\infty}$ respectively. Then the only freedom in determining the optimal bases

[1] Geometrically, "the same" means two surfaces are isometric to each other

is the sign of the eigenfunctions. If we write $\Gamma = \{\gamma = (\gamma_0, \gamma_1, \cdots) \mid \gamma_i \in \{1, -1\}\}$ and $\tilde{\Phi}_\gamma = \{(\tilde{\lambda}_i, \gamma_i \tilde{\phi}_i)\}_{i=0}^{\infty}$, the spectral l^2-distance will have the following form:

$$d(\mathcal{M}, \tilde{\mathcal{M}}) = \inf_{\gamma \in \Gamma} \max \Big\{ \int_{\mathcal{M}} d_{\Phi}^{\tilde{\Phi}_\gamma}(x, \tilde{\mathcal{M}}) \mathrm{d}_{\mathcal{M}}(x) \, , \int_{\tilde{\mathcal{M}}} d_{\Phi}^{\tilde{\Phi}_\gamma}(\mathcal{M}, y) \mathrm{d}_{\tilde{\mathcal{M}}}(y) \Big\} \tag{3.1}$$

This shows that the computation of the spectral l^2-distance is a combinatorial optimization problem for surfaces with simple eigen-systems. It is numerically intractable to compute infinite number of eigenfunctions to obtain the exact embedding defined in (2.10). However, since $\{\phi_i(x)/\sqrt{\lambda_i}\}_{i=1}^{\infty}$ is convergent, we can approximate the spectral l^2-distance to the theoretical definition using the first n LB eigenfunctions in the following way.

Let us write

$$I_{\mathcal{M}}^{\Phi(n)}(x) = \left(\frac{\phi_i(x)}{\sqrt{\lambda_i}} \right)_{i=1}^{n} \in \mathbb{R}^n, \quad I_{\tilde{\mathcal{M}}}^{\tilde{\Phi}_\gamma(n)}(x) = \left(\frac{\gamma_i \tilde{\phi}_i(x)}{\sqrt{\tilde{\lambda}_i}} \right)_{i=1}^{n} \in \mathbb{R}^n$$

$$d_{\Phi(n)}^{\tilde{\Phi}(n)}(x, \tilde{\mathcal{M}}) = \min_{y \in \tilde{\mathcal{M}}} ||I_{\mathcal{M}}^{\Phi(n)}(x) - I_{\tilde{\mathcal{M}}}^{\tilde{\Phi}_\gamma(n)}(y)||_2 \, , \ \forall \ x \in M$$

$$d_{\Phi(n)}^{\tilde{\Phi}\gamma(n)}(\mathcal{M}, y) = \min_{x \in \mathcal{M}} ||I_{\mathcal{M}}^{\Phi(n)}(x) - I_{\tilde{\mathcal{M}}}^{\tilde{\Phi}_\gamma(n)}(y)||_2 \, , \ \forall \ y \in \tilde{\mathcal{M}}$$

The first n LB eigenfunctions can define a distance:

$$d_n(\mathcal{M}, \tilde{\mathcal{M}}) = \inf_{\gamma \in \Gamma(n)} \max \Big\{ \int_{\mathcal{M}} d_{\Phi(n)}^{\tilde{\Phi}_\gamma(n)}(x, \tilde{\mathcal{M}}) \mathrm{d}_{\mathcal{M}}(x) \, , \int_{\tilde{\mathcal{M}}} d_{\Phi(n)}^{\tilde{\Phi}_\gamma(n)}(\mathcal{M}, y) \mathrm{d}_{\tilde{\mathcal{M}}}(y) \Big\} \tag{3.2}$$

where $\Gamma(n) = \Big\{ \gamma = (\gamma_0, \gamma_1, \cdots, \gamma_n) \mid \gamma_i \in \{1, -1\}, i = 0, 1, \cdots, n \Big\}$.

Numerically, two surfaces are represented by triangle meshes $\mathcal{M} = \Big\{ V = \{v_i\}_{i=1}^{N}, T = \{T_l\}_{l=1}^{L} \Big\}$ and $\tilde{\mathcal{M}} = \Big\{ \tilde{V} = \{\tilde{v}_i\}_{i=1}^{\tilde{N}}, \tilde{T} = \{\tilde{T}_l\}_{l=1}^{\tilde{L}} \Big\}$. We denote the embedding images of vertices by $\Big\{ w_i = I_{\mathcal{M}}^{\Phi(n)}(v_i) \Big\}_{i=1}^{N}$ and $\Big\{ \tilde{w}_i = I_{\tilde{\mathcal{M}}}^{\tilde{\Phi}(n)}(\tilde{v}_i) \Big\}_{i=1}^{\tilde{N}}$ respectively, then the corresponding triangle meshes of their LB embedding images can be represented by $I_{\mathcal{M}}^{\Phi(n)}(\mathcal{M}) = \Big\{ I_{\mathcal{M}}^{\Phi(n)}(V) = \{w_i\}_{i=1}^{N}, T = \{T_l\}_{l=1}^{L} \Big\}$ and $I_{\tilde{\mathcal{M}}}^{\tilde{\Phi}(n)}(\tilde{\mathcal{M}}) = \Big\{ I_{\tilde{\mathcal{M}}}^{\tilde{\Phi}(n)}(\tilde{V}) = \{\tilde{w}_i\}_{i=1}^{\tilde{N}}, \tilde{T} = \{\tilde{T}_l\}_{l=1}^{\tilde{L}} \Big\}$. We approximate the distance $d_n(\mathcal{M}, \tilde{\mathcal{M}})$ as follows:

$$\begin{aligned} d_{\Phi(n)}^{\tilde{\Phi}(n)}(v_i, \tilde{\mathcal{M}}) &= \min_{y \in \tilde{\mathcal{M}}} ||I_{\mathcal{M}}^{\Phi(n)}(v_i) - I_{\tilde{\mathcal{M}}}^{\tilde{\Phi}_\gamma(n)}(y)||_2, \\ &\approx \min_{\tilde{T}_l = (l_1, l_2, l_3) \in \tilde{T}} \min_{\substack{\alpha_1, \alpha_2, \alpha_3 \geq 0 \\ \alpha_1 + \alpha_2 + \alpha_3 \leq 1}} ||w_i - (\alpha_1 \tilde{w}_{l_1} + \alpha_2 \tilde{w}_{l_2} + \alpha_3 \tilde{w}_{l_3})||_2 \end{aligned} \tag{3.3}$$

The integral on $\mathcal{M}$ can be approximated by:

$$\int_{\mathcal{M}} d_{\Phi(n)}^{\tilde{\Phi}_\gamma(n)}(x, \tilde{\mathcal{M}}) \mathrm{d}_{\mathcal{M}}(x) \approx \frac{1}{area(\mathcal{M})} \sum_{i=1}^{N} d_{\Phi(n)}^{\tilde{\Phi}_\gamma(n)}(v_i, \tilde{\mathcal{M}}) \cdot A_i \tag{3.4}$$

where $A_i = \frac{1}{3} \sum_{v_i \in T_l} area(T_l)$.

Similarly, we have:

$$\begin{aligned} d_{\Phi(n)}^{\tilde{\Phi}(n)}(\mathcal{M}, \tilde{v}_i) &= \min_{x \in \tilde{\mathcal{M}}} ||I_{\mathcal{M}}^{\Phi(n)}(x) - I_{\tilde{\mathcal{M}}}^{\tilde{\Phi}_\gamma(n)}(\tilde{v}_i)||_2, \\ &\approx \min_{T_l = (l_1, l_2, l_3) \in T} \min_{\substack{\alpha_1, \alpha_2, \alpha_3 \geq 0 \\ \alpha_1 + \alpha_2 + \alpha_3 \leq 1}} ||(\alpha_1 w_{l_1} + \alpha_2 w_{l_2} + \alpha_3 w_{l_3}) - \tilde{w}_i||_2 \end{aligned} \tag{3.5}$$

$$\int_{\tilde{\mathcal{M}}} d^{\tilde{\Phi}_{\gamma}(n)}_{\Phi(n)}(\mathcal{M}, y)\mathrm{d}_{\mathcal{M}}(y) \approx \frac{1}{area(\tilde{\mathcal{M}})} \sum_{i=1}^{\tilde{N}} d^{\tilde{\Phi}_{\gamma}(n)}_{\Phi(n)}(\mathcal{M}, \tilde{v}_i) \cdot \tilde{A}_i \tag{3.6}$$

where $\tilde{A}_i = \frac{1}{3}\sum_{v_i \in \tilde{T}_l} area(\tilde{T}_l)$.

To demonstrate the approximated distance and its ability of picking the optimal embedding bases for shape analysis, we show in Fig. 3.1 the embedding of two cortical surfaces with the first three eigenfunctions. Out of the eight possible embeddings, the one achieving the distance $d_3(\mathcal{M}, \tilde{\mathcal{M}})$ is highlighted inside the red circle. While the right cortical surface with red color and the left cortical surface with green color have significantly different poses in the Euclidean space, their embedding are very close to each other, which reflects the fact that these two surfaces share very similar intrinsic geometry. This example clearly illustrates the power of the optimal embedding in characterizing the intrinsic geometry of surfaces.

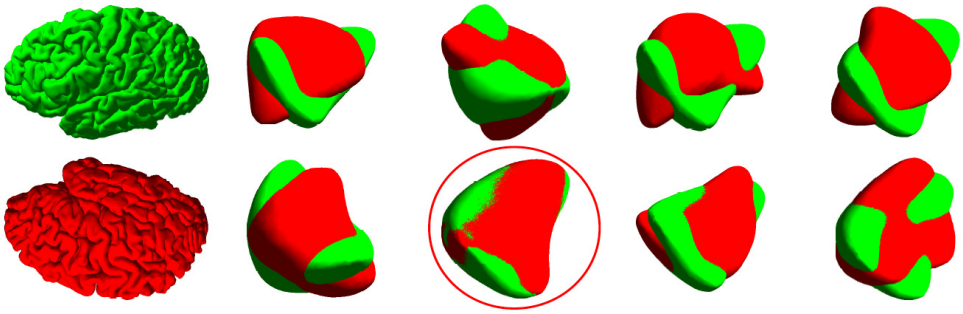

FIG. 3.1. *The first column: two input surfaces for computing their spectral l^2-distance.The last four columns: 8 possible embedding due to sign ambiguity of the first three eigenfunctions.*

Since the spectral l^2-distance actually is dominated by the first n eigenfunctions, the optimal embedding bases of $d_n(\cdot,\cdot)$ will be the first n bases functions of the optimal embedding bases of the spectral l^2-distance. Therefore, we just need to compute $d_n(\cdot,\cdot)$ to approximate the spectral l^2-distance $d(\cdot,\cdot)$ and obtain the first n eigenfunctions of the optimal embedding bases. However, the complexity of the combinatorial optimization problem (3.2) to compute $d_n(\cdot,\cdot)$ is still 2^n. Based on the fact that the sequences $\{\phi_i(x)/\sqrt{\lambda_i}\}_{i=1}^{\infty}$ and $\{\tilde{\phi}_i(x)/\sqrt{\tilde{\lambda}_i}\}_{i=1}^{\infty}$ rapidly converge to zero, we propose to recursively optimize $d_n(\cdot,\cdot)$ and obtain the optimal embedding bases, which is described by the the following **Frequency Band-wise Search** (FBS) approach.

Algorithm (Frequency Band-wise Search):

1. Fix a number n_0, we compute $d_{n_0}(\cdot,\cdot)$ to obtain $(\gamma_0, \gamma_1, \cdots, \gamma_{n_0})$ of the first n_0 components of the optimal embedding bases by optimize the problem (3.2) with exhaustive search;
2. For a positive integer p, suppose $d_{pn_0}(\cdot,\cdot)$ has been computed with the first pn_0 components of the optimal embedding bases. Then $d_{(p+1)n_0}(\cdot,\cdot)$ is computed by fixing the first pn_0 components of the optimal embedding bases and searching the rest $pn_0 + 1, \cdots, (p+1)n_0$ bases.

In practice, n_0 is chosen to be a small integer such as 3 or 4. Given a number n, we first write n as $k * n_0 + m$ with $0 \le m < n_0$. Then, $d_n(\cdot,\cdot)$ and the corresponding optimal embedding bases are recursively computed by the above FBS approach. With this approach, the combinatorial optimization problem (3.2) with complexity 2^n can be dramatically simplified

and approximated by $k+1$ subproblems with total complexity $(k+1)2^{n_0}$. To check the robustness of the proposed FBS algorithm, we conduct experiments of computing $d_{15}(\cdot,\cdot)$ from a hippocampus surface to several other surfaces with different geometry. The complexity of the true combinatorial optimization problem is 2^{15}, which is very time consuming with the exhausted search method. However, the computation cost can be decreased to 5×2^3 with $n_0 = 3$ or, $3 \times 2^4 + 2^3$ with $n_0 = 4$ using the proposed FBS method. In Table 3.1, we illustrate the efficiency and accuracy of the proposed FBS algorithm to compute $d_{15}(\cdot,\cdot)$. The error here is naturally defined by

$$\textbf{error} = \frac{\text{True value from exhausted search} - \text{Results from FBS}}{\text{True value from exhausted search}}.$$

By comparing with the results obtained by exhausted search requiring hours of computation, it is clear to see that the FBS algorithm provides us a very efficient and accurate method to approximate the spectral l^2-distance.

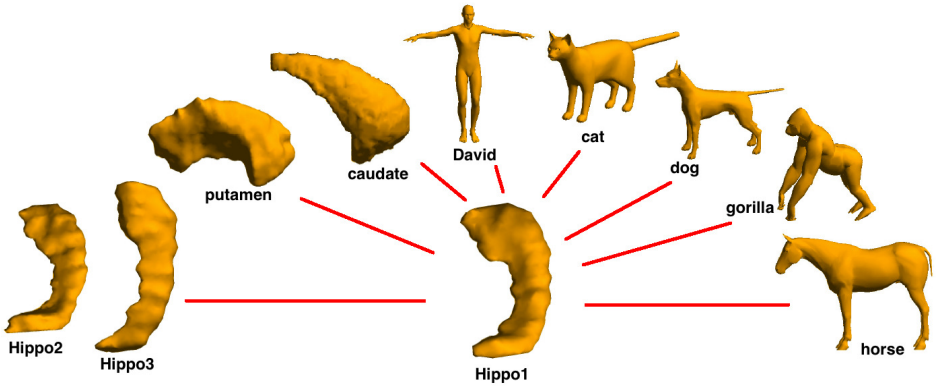

TABLE 3.1
Comparison of spectral l^2-distance obtained by FBS with true value obtained by exhausted search

	Spectral l^2-distance to Hippocampus 1							
	True value by exhausted search		The proposed FBS algorithm					
			n_0 = 3			n_0 = 4		
	distance	time (h:m:s)	distance	time (s)	error	distance	time (s)	error
Hippo2	0.0391	6:54:28	0.0391	2.502	0.0	0.0391	3.406	0.0
Hippo3	0.0322	6:51:14	0.0322	2.544	0.0	0.0322	3.426	0.0
Puteman	0.1603	20:43:26	0.1640	7.596	2.31%	0.1614	10.200	0.69%
Caudate	0.1460	10:08:14	0.1474	3.840	0.96%	0.1474	5.593	0.96%
david	0.4571	16:58:02	0.4571	8.526	0.0	0.4571	11.650	0.0
cat	0.2436	16:55:27	0.2463	8.258	1.11%	0.2436	11.386	0.0
dog	0.3349	16:49:02	0.3349	8.388	0.0	0.3349	11.607	0.0
gorilla	0.3337	9:30:11	0.3525	4.722	5.6%	0.3337	6.536	0.0
horse	0.3392	16:54:17	0.3392	8.328	0.0	0.3392	11.366	0.0

Because the spectral l^2-distance depends completely on the intrinsic geometry of surfaces, we expect intuitively its value will reflect the similarity between surfaces. In other words, as a global quantity, the spectral l^2-distance can provide us a useful tool to intrinsically characterize surface differences. Inspired by this observation, a valuable application of proposed spectral l^2-distance is to study surface classification problems, which will be discussed in more detail in Section 4.

Moreover, the spectral l^2-distance does not only provide us global quantities to classify surfaces, but also will provide us tools to conduct local surface comparison, which is

the biggest distinction of our proposed approach from other feature-based approaches [43, 1, 34, 57] or shape space-based approaches [25], Notice that the definition of our spectral l^2-distance is coming from the scale invariant embedding obtained by LB eigensystems, which means the optimal embedding bases can be obtained as co-products of the spectral l^2-distance. With the spectral l^2-distance and the resulting optimal embedding bases, we can compare surfaces locally in the common embedding space. This is a critical component in many different applications such as identifying meaningful and stable parts across a large group of surfaces with similar intrinsic geometry, constructing correspondences between surfaces. In the following sections about applications of the spectral l^2-distance, we will demonstrate how to utilize the proposed framework to conduct surface classification, surface feature identification and surface mapping.

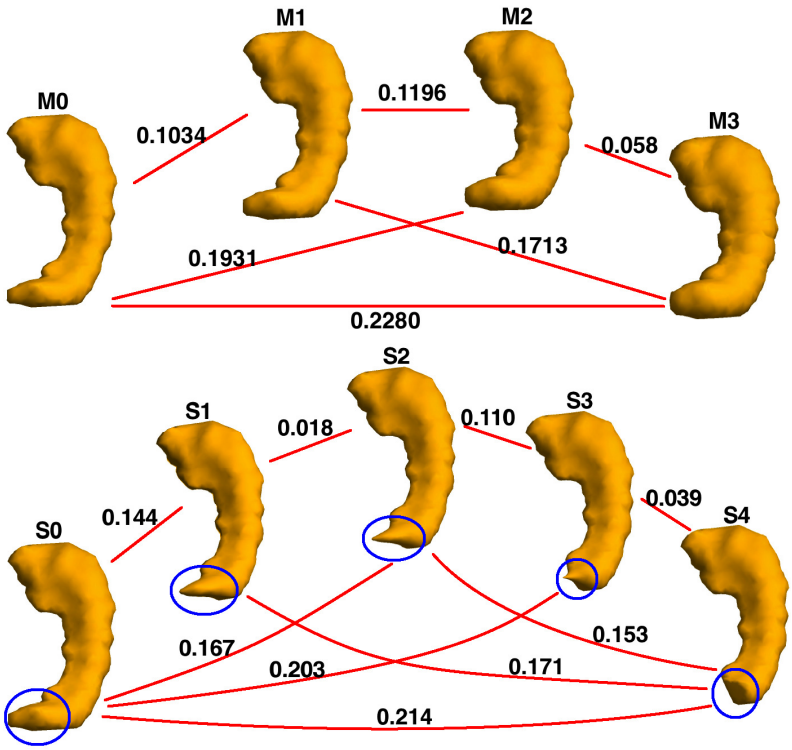

FIG. 4.1. *Pairwise spectral l^2-distance under global inflation (the first row) and local shrinkage (the second row). The blue circles in the second row mark the local shrinkages*

4. Application I: Surface Similarity Measurement. Due to the theorem 2.5, the proposed spectral l^2-distance will reflect the intrinsic surface geometry. To illustrate the geometric meaning of the spectral l^2-distance, we demonstrate in three experiments how the proposed distance can help us to describe either local or global surface difference.

In our first two synthetic examples, we consider two groups of surfaces obtained from global and local deformation respectively, which are two cases usually considered in medical imaging due to certain disease induced anatomic structure deformations. In this example, a hippocampus surface obtained from the magnetic resonance image of a human brain is considered as the initial surface. As shown in Figure. 4.1, global inflations and local shrinkage operations were applied to the hippocampus to generate synthetic examples for analysis.

Global inflations are generated via outward deformation along normal directions, and local shrinkages are genarated via inward deformation along normal directions in regions highlighted with blue circles. Shapes in both groups are ordered with increased degree of deformation from left to right. We compute the proposed spectral l^2-distance by calculating its approximation with the first 20 LB eigenfunctions using the FBS method with $n_0 = 4$ as discussed in last section. Pairwise spectral l^2-distances of surfaces in each group are labeled in Figure. 4.1. From the pairwise distances shown in Figure. 4.1, it is clear that the proposed distance is compatible with the geometric intuition. For instance, the spectral l^2-distance captures the increasing shape difference from $M0$ to $M1$, $M2$ and $M3$. A similar trend can be observed in the examples generated via local shrinkages. Overall we can see surfaces with more similar shapes have smaller spectral l^2-distances.

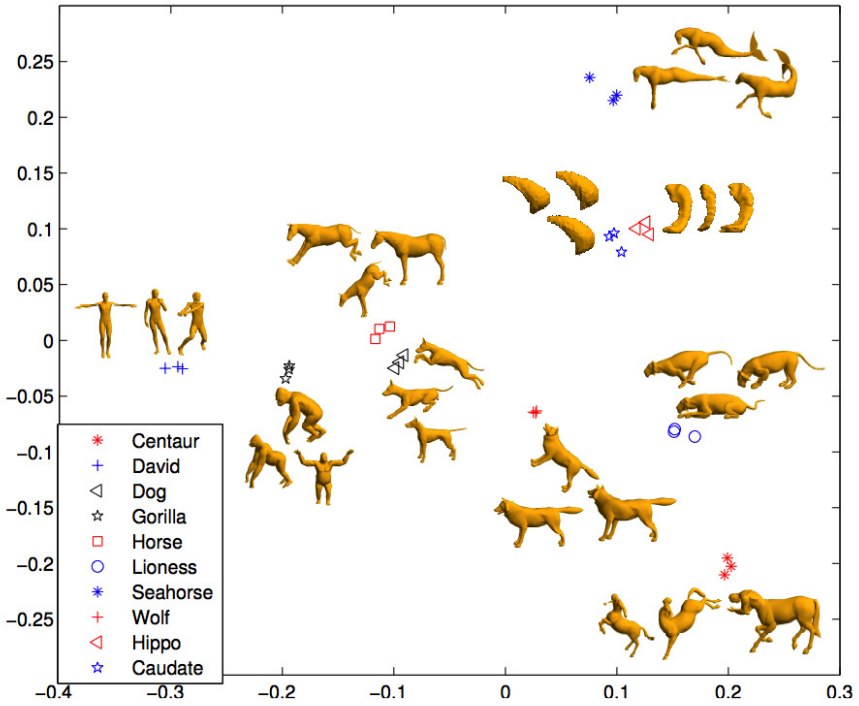

FIG. 4.2. *MDS embedding results with the spectral l^2-distance.*

To further demonstrate the ability of spectral l^2-distance in surface global geometry detection, we apply the spectral l^2-distance to classify 30 different surfaces. Three human, three dogs, three gorilla, three lioness, three horses, three seahorses, three wolves and three centaur surfaces with different poses are from public available data base TOSCA [5, 7, 8] and three hippocampus and three caudate surfaces are from LONI in UCLA. In this experiment, we choose the first 20 LB eigenvalues and eigenfunctions to approximate the spectral l^2-distance. To visualize the embedding, we utilize the multi-dimension scaling(MDS) [4] technique to project these surfaces into a 2D plane as shown in Fig. 4.2. It clearly shows that surfaces with similar intrinsic geometry cluster together under the spectral l^2-distance.

5. Application II: Sulci Identification on Vervet Cortical Surfaces. In this section, we apply our spectral l^2-distance to the problem of automated sulci identification in 3D med-

ical image analysis. The identification of major sulci is one of the critical steps in cortical surface analysis [54]. However, the manual labeling of sulcal regions becomes impractical with the increasing availability of large data set. Therefore, it is important to find a robust way to identify the major sulci automatically. In this section, we develop a robust approach to identify sulcal regions based on the spectral l^2-distance. To demonstrate our method, we further apply the algorithm in a real data set, vervet cortical surfaces provided by S. Fears and R. P. Woods [19, 62].

To identify sulcal regions of a given cortical surface, the first step is to parcellate the cortical surface into sulcal and gyral regions. Using the mean curvature as an image defined on the surface, we extend the convexified version of Chan-Vese(CV) [13, 12] model to 3D triangulated surfaces for the extraction of sulcal regions [30]. Let $I : M \to \mathbb{R}$ be an image

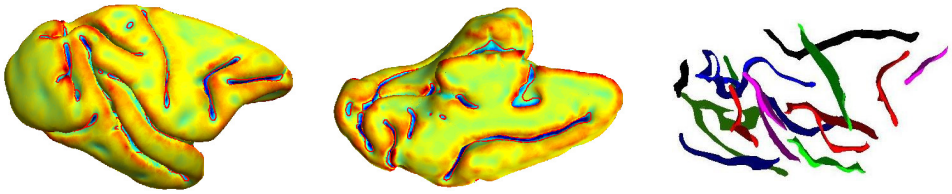

(a) (b) (c)

FIG. 5.1. *(a), (b): two different views of CV segmentation. The surfaces are color coded with its mean curvature and the red contours mark the boundary of the sulcal and gyral regions. (c): sulcal regions obtained by the CV segmentation model on the cortical surface.*

on a surface $\mathcal{M}$. The parcellation of the cortical surfaces then can be obtained by solving the following convexified version of CV segmentation model on $\mathcal{M}$;

$$arg \min_{\substack{0\leqslant u\leqslant 1\\ c1,c2}} \left(\int_{\mathcal{M}} |\nabla_{\mathcal{M}} u| + \mu \int_{\mathcal{M}} u((c_1 - I)^2 - (c_2 - I)^2) \right) \tag{5.1}$$

In Fig. 5.1, we show the segmentation result obtained by applying the CV segmentation model to a vervet cortex. The resultant of sulcal regions are also shown.

Because all cortical surfaces share similar geometry, they will cluster together in the embedding space determined by the spectral l^2-distance. As we illustrated in section 3, these surfaces overlap quite well in the embedding space. For major sulci on cortical surfaces, their relative positions on the cortex are stable and so are their locations in the embedding space. This suggests that the same sulcal line from different cortical surfaces will form clusters in the embedding space.

Assuming we have a large group of cortical surfaces, we use template matching to build an automated approach to label sulci on vervet cortical surfaces. Let $\mathcal{M}$ denote a template cortical surface that has a set of manually labeled sulci to be identified. For an arbitrary vervet cortical surface $\tilde{\mathcal{M}}$, we find the major sulci on $\tilde{\mathcal{M}}$ by comparing it with $\mathcal{M}$ in the embedding space determined by the spectral l^2-distance. The detailed algorithm for the automated sulcal identification process is as follows:

1. Use the CV segmentation model to extract sulcal regions for both $\mathcal{M}$ and $\tilde{\mathcal{M}}$. Let the sulcal regions of $\mathcal{M}, \tilde{\mathcal{M}}$ be denoted by $\{l_1, \cdots, l_k\}, \{\tilde{l}_1, \cdots, \tilde{l}_{\tilde{k}}\}$, respectively. For the template cortical surface $\mathcal{M}$, the labeling of its sulci is known *a priori*.
2. Choose a suitable number n, compute $d_n(\cdot, \cdot)$ as a numerical approximation of the spectral l^2-distance between $\mathcal{M}$ and $\tilde{\mathcal{M}}$ to obtain the optimal embedding bases $\{\phi_i/\sqrt{\lambda_i}\}_{i=1}^n, \{\tilde{\phi}_i/\sqrt{\tilde{\lambda}_i}\}_{i=1}^n$ for $\mathcal{M}, \tilde{\mathcal{M}}$ respectively.

3. To identify the sulcal regions $\{\tilde{l}_1, \cdots, \tilde{l}_{k'}\}$ of $\tilde{\mathcal{M}}$, we compute the sulcal region correspondence $\sigma : \{\tilde{l}_1, \cdots, \tilde{l}_{\tilde{k}}\} \to \{l_1, \cdots, l_k\}$. For each sulcal region l'_j of the target surface $\tilde{\mathcal{M}}$, we compute its spectral pre-l^2-distance in the embedding space to each sulcal region of $\mathcal{M}$ with respect to $\{\phi_i/\sqrt{\lambda_i}\}, \{\tilde{\phi}_i/\sqrt{\tilde{\lambda}_i}\}$. We label l'_j to a sulcal region $\sigma(\tilde{l}_j)$ of $\mathcal{M}$ who attains the shortest distance to $\tilde{l}_j$.

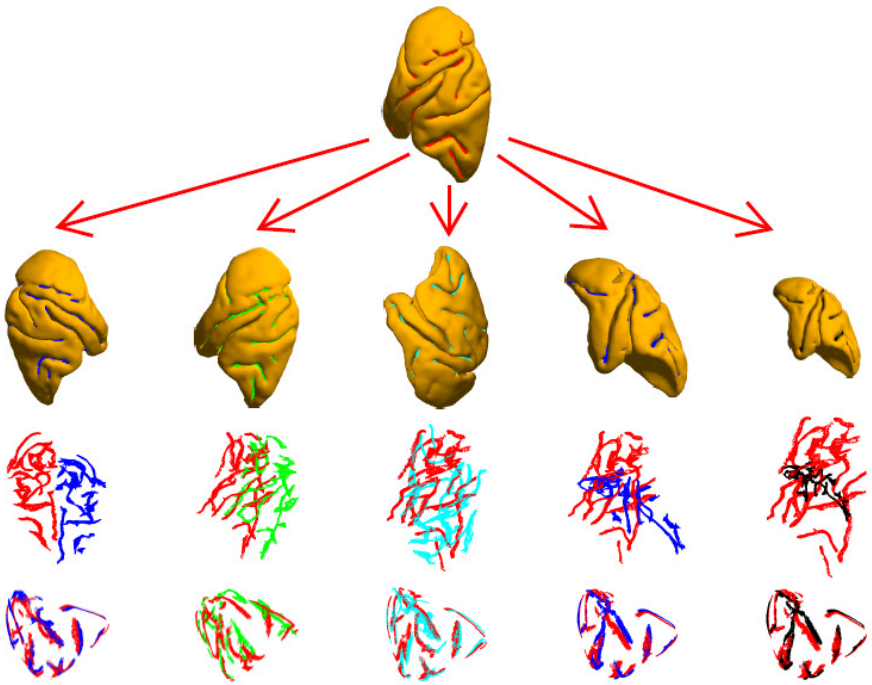

FIG. 5.2. *The first row: the template cortical surface with sulcal regions marked in red; the second row: target cortical surfaces with sulcal regions marked by different colors; the third row: sulcal regions of the template and target cortical surfaces in the Euclidean space; the fourth row: sulcal regions of the template and target cortical surfaces in the embedding space.*

In our experiment, we illustrate the pose and scale invariance of our method by comparing a template brain and five other brains with different poses and scales. The results are shown in Fig 5.2. To visualize the embedding images of two surfaces, we choose the first three eigenfunctions and compute $d_3(\cdot, \cdot)$ to obtain the optimal embedding bases. The five surfaces shown in the second row have various pose and scales differences in the Euclidean space as compared to the template. As shown in the third row, the positions of similar sulci in the Euclidean spaces are misaligned. However, similar sulci will automatically cluster together in the embedding space under the optimal basis as shown in the fourth row. This demonstrates that the spectral l^2-distance and the embedding based on its associated optimal basis reflect intrinsic geometry and they are rotation, translation and scale invariant.

6. Application III: Direct Surface Mapping. The problem of surface mapping considers the construction of meaningful correspondences among surfaces with complicated geometric structures. It has applications in various problems including measuring non-rigid geometric difference in computer graphics [6, 64], and mapping structures in brain imaging study [53, 61, 50, 63, 35]. Generally surface maps are computed on parameterization domains [65, 35]. Given two surfaces $\mathcal{M}$ and $\tilde{\mathcal{M}}$, they are first parametrized on a simple domain D

such as the plane, the sphere, or a coarse simplicial domain to obtain two parametrization maps $\pi : \mathcal{M} \to D$ and $\pi' : \tilde{\mathcal{M}} \to D$. Then a selfmap $\rho : D \to D$ can be introduced to adjust the overall correspondence which is represented by $\Pi = \pi'^{-1} \circ \rho \circ \pi : \mathcal{M} \to \tilde{\mathcal{M}}$. However, parametrization is a challenge problem for a general surfaces and may introduce inaccuracy for surfaces with complicated geometry. As the third application, our spectral l^2-distance can be further utilized to the problem of surface mapping. The biggest advantage of the new approach proposed here is that the correspondences are directly constructed between two surfaces without the need of parameterization.

Assuming we have two surfaces $\mathcal{M}$ and $\tilde{\mathcal{M}}$, we introduce the following procedure to construct surface mapping using the spectral l^2-distance.

1. By choosing a suitable n, we first compute $d_n(\cdot,\cdot)$ as the approximation of spectral l^2-distance between $\mathcal{M}$ and $\tilde{\mathcal{M}}$ to obtain the optimal embedding bases $\{\phi_i/\sqrt{\lambda_i}\}_{i=1}^n$, and $\{\tilde{\phi}_i/\sqrt{\tilde{\lambda}_i}\}_{i=1}^n$, for $\mathcal{M}$ and $\tilde{\mathcal{M}}$ respectively.
2. As we discussed in the proof of lemma 2.7, for any point $x \in M$, we define its corresponding point in $\tilde{\mathcal{M}}$ by

$$y_x = arg \min_{y \in \tilde{\mathcal{M}}} ||I^{\Phi}_{\mathcal{M}}(x) - I^{\tilde{\Phi}}_{\tilde{\mathcal{M}}}(y)||_2 \tag{6.1}$$

Similarly, for any point $y \in \tilde{\mathcal{M}}$, we define its corresponding points in $\mathcal{M}$ by

$$x_y = arg \min_{x \in \mathcal{M}} ||I^{\Phi}_{\mathcal{M}}(x) - I^{\tilde{\Phi}}_{\tilde{\mathcal{M}}}(y)||_2 \tag{6.2}$$

Therefore, we have two maps $f : \mathcal{M} \to \tilde{\mathcal{M}} \quad x \longmapsto y_x$ and $f' : \tilde{\mathcal{M}} \to \mathcal{M} \quad y \longmapsto x_y$. Note that for two triangulated surfaces $\mathcal{M} = \{V = \{v_i\}_{i=1}^N, T = \{T_l\}_{l=1}^L\}$ and $\tilde{\mathcal{M}} = \{\tilde{V} = \{\tilde{v}_i\}_{i=1}^{\tilde{N}}, \tilde{T} = \{\tilde{T}_l\}_{l=1}^{\tilde{L}}\}$, the correspondence is not necessarily vertex to vertex. The surface embeddings in l^2 we consider are not only the embedding of vertices but also the embedding of interior points of each triangle. Therefore, the correspondence of each vertex in source surface $\mathcal{M}$ might be an interior point of certain triangle on the target surface $\tilde{\mathcal{M}}$.

Using this algorithm, we can directly compute the correspondences between surfaces without the need of parameterization. Due to the optimal embedding bases, the resulting map can automatically capture the geometric information of two surfaces, i.e., patches having similar geometry on two surfaces will be mapped to each other. Due to the intrinsic properties of LB eigen-systems, the mapping algorithm depends only on the intrinsic geometry of source and target surfaces. It is rotation, translation, scale and pose invariant.

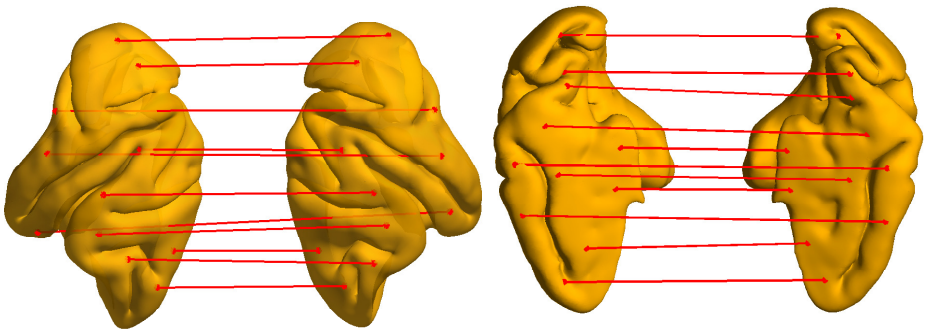

FIG. 6.1. *Two views of the constructing map between a left vervet cortical surface and a right vervet cortical surface.*

To illustrate our surface mapping method, we demonstrate in two experiments the construction of correspondences among anatomic structures. In the first experiment, we compute correspondences between two vervet cortical surfaces. The approximation of spectral l^2-distance used for this experiment is $d_{30}(\cdot,\cdot)$. These two vervet cortical surfaces are from the same vervet brain, one is the left cortical surface and the other is the right cortical surface. Therefore, they have very close intrinsic geometry but different Euclidean coordinate representations. As shown in Fig. 6.1, accurate surface mapping can be established with our method even though the Euclidean representation of these two surfaces are quite different.

In brain image analysis, it is critical to consider the correspondence between white and gray matter surfaces. Meaningful correspondences could be further used to cortex analysis such as studying cortex thickness, detecting cortex cellular layers, etc. However, the highly folded sulcal and gyral structures make it a difficult task to map the white matter and gray matter surfaces in the Euclidean domain. To tackle this problem, we apply our direct surface mapping approach using $d_{30}(\cdot,\cdot)$ to approximate the spectral l^2-distance. The correspondences between the white matter surface and the gray matter surface are illustrated in Fig. 6.2. It is clear to see that our mapping algorithm successfully establishes sulci-to-sulci and gyri-to-gyri correspondences between these two highly complicated surfaces.

7. Conclusions. In summary, we proposed a general framework for surface global and local analysis by constructing a mathematically rigorous distance, spectral l^2-distance, on shape space based on surface Laplace-Beltrami eigen-systems. This distance captures the intrinsic geometry of surfaces, which is robust to translation, rotation, scale and pose variations. Compared with other distance measures of surfaces, one distinct feature of the spectral l^2-distance is that it provides a pair of optimal embedding bases on two surfaces. The combination of the spectral l^2-distance and its induced optimal embedding bases enables us to compare surfaces in both local and global perspectives. To demonstrate applications of the proposed spectral l^2-distance, we first illustrate its application in surface classification. We also developed a robust approach to identify major sulci on vervet cortical surfaces, which are salient local features on complicated surfaces. Finally, we proposed a direct surface mapping algorithm and illustrated its application in computing detailed correspondences between cortical surfaces.

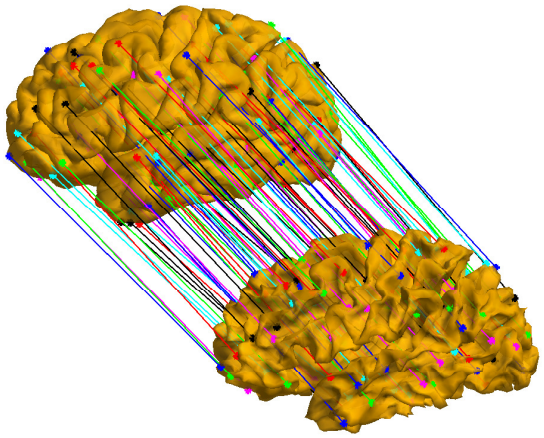

FIG. 6.2. *An illustration of the map between a white matter and gray matter surface.*

Acknowledgment. Rongjie Lai's work is supported by Zumberge Individual Award from USC's James H. Zumberge Faculty Research and Innovation Fund. Yonggang Shi's work was partially supported by NIH grants 5P41RR013642. Authors would like to express their gratitude to Prof. Roger P. Woods and Prof. Scott Fears for providing the vervet cortical surfaces database.

REFERENCES

[1] S. BELONGIE, J. MALIK, AND J. PUZICHA, *Shape matching and object recognition using shape contexts*, IEEE Trans. Pattern Anal. Machine Intell., 24 (2002), pp. 509–522.

[2] M. BEN-CHEN AND C. GOTSMAN, *Characterizing shape using conformal factors*, Proceedings of Eurographics Workshop on Shape Retrieval, (Crete, April, 2008).

[3] P. BÉRARD, G. BESSON, AND S. GALLOT, *Embedding riemannian manifolds by their heat kernel*, Geom. Funct. Anal., 4 (1994), pp. 373–398.

[4] I. BORG AND P. GROENEN, *Modern Multidimensional Scaling: theory and applications*, Springer-Verlag New York, 2nd ed., 2005.

[5] A. M. BRONSTEIN, M. M. BRONSTEIN, AND R. KIMMEL, *Efficient computation of isometry-invariant distances between surfaces*, SIAM Journal of Scientific Computing, 28 (2006), pp. 1812–1836.

[6] ———, *Generalized multidimensional scaling: a framework for isometry-invariant partial surface matching*, Proc. Nat. Acad. Sci. U.S.A., 103 (2006), pp. 1168–1172.

[7] ———, *Calculus of non-rigid surfaces for geometry and texture manipulation*, IEEE Trans. Visualization and Computer Graphics, 13 (2007), pp. 902–913.

[8] ———, *Numerical geometry of non-rigid shapes*, Springer, (2008).

[9] A. M. BRONSTEIN, M. M. BRONSTEIN, R. KIMMEL, M. MAHMOUDI, AND G. SAPIRO, *A gromov-hausdorff framework with diffusion geometry for topologically-robust non-rigid shape matching*, Int. Jour. Comput. Vis., 89 (2010), pp. 266–286.

[10] M. M. BRONSTEIN AND I. KOKKINOS, *Scale-invariant heat kernel signatures for non-rigid shape recognition*, Proc. Computer Vision and Pattern Recognition (CVPR), (2010).

[11] D. BURAGO, Y. BURAGO, AND S. IVANOV, *A course in metric geometry*, Graduate studies in mathematics, AMS, 33 (2001).

[12] T. F. CHAN, S. ESEDOGLU, AND M. NIKOLOVA, *Algorithms for finding global minimizers of image segmentation and denoising models*, SIAM Journal on Applied Mathematics, 66 (2006), pp. 1632–1648.

[13] T. F. CHAN AND L. VESE, *Active contours without edges*, IEEE Transactions on Image Processing, 10 (2001), pp. 266–277.

[14] I. CHAVEL, *Eigenvalues in Riemannian Geometry*, Academic press. INC, 1984.

[15] R. R. COIFMAN AND S. LAFON, *Diffusion maps*, Applied and Computational Harmonic Analysis, 21 (2006).

[16] T. COOTES, C. TAYLOR, D. COOPER, AND J. GRAHAM, *Active shape models -their training and application*, Computer Vision and Image Understanding, 61 (1995), pp. 38–59.

[17] S. DONG, P-T. BREMER, M. GARLAND, V. PASCUCCI, AND J. C. HART, *Spectral surface quadrangulation*, ACM Transactions on Graphics (TOG) - Proceedings of ACM SIGGRAPH, (2006).

[18] A. ELAD AND R. KIMMEL, *On bending invariant signatures for surfaces*, IEEE Trans. Pattern Anal. Machine Intell., 25 (2003), pp. 1285–1295.

[19] S. C. FEARS, W. P. MELEGA, S.K. SERVICE, C. LEE, K. CHEN, Z. TU, M. J. JORGENSEN, L. A. FAIRBANKS, R. M. CANTOR, N.B. FREIMER, AND R. P. WOODS, *Identifying heritable brain phenotypes in an extended pedigree of vervet monkeys*, J. Neurosci., 29 (2009), pp. 2867–2875.

[20] T. FUNKHOUSER, P. MIN, M. KAZHDAN, J. CHEN, A. HALDERMAN, D. DOBKIN, AND D. JACOBS, *A search engine for 3D models*, ACM Trans. Graph., 22 (2003), pp. 83–105.

[21] C. GORDON, D. WEBB, AND S. WOLPERT, *One cannot hear the shape of a drum*, Bull. Am. Math.Soc., 27 (1992), pp. 134–138.

[22] X. GU, Y. WANG, T. F. CHAN, P. THOMPSON, AND S. T. YAU, *Genus zero surface conformal mapping and its application to brain surface mapping*, IEEE Transaction on Medical Imaging, 23 (2004), pp. 949–958.

[23] D. JANKOBSON, N. NADIRASHBILI, AND J. TOTH, *Geometric propertiess of eigenfunctions*, Russian Math. Surveys, 56 (2001), pp. 1085–1105.

[24] M. JIN, F. LUO, S. YAU, AND X. GU, *Computing geodesic spectra of surfaces*, Proc. ACM Symposium on Solid and Physical Modeling, (2007), pp. 387–393.

[25] M. JIN, W. ZENG, F. LUO, AND X. GU, *Computing Teichmüller shape space*, IEEE Transaction on Visualization and Computer Graphics, 15 (2009), pp. 504–517.

[26] P. W. JONES, M. MAGGIONI, AND R. SCHUL, *Manifold parametrizations by eigenfunctions of the laplacian and heat kernels*, Proc Natl Acad Sci U S A, 105 (2008), pp. 1803–1808.

[27] J. JOST, *Riemannian geometry and geometric analysis*, Springer, 3rd edition, (2001).

[28] M. KAC, *Can one hear the shape of a drum?*, Am Math Mon, 73(4) (1966), pp. 1–23.

[29] S. LAFON, *Diffusion Maps and Geometric Harmonics*, PhD thesis, Yale University, 2004.

[30] R. LAI AND T. F. CHAN, *A framework for intrinsic image processing on surfaces*, Computer Vision and Image Understanding, 115 (2011), pp. 1647–1661.

[31] R. LAI, Y. SHI, I. DINOV, T. F. CHAN, AND A. W. TOGA, *Laplace-beltrami nodal counts: a new signature for 3d shape analysis*, in Proc. ISBI, 2009, pp. 694–697.

[32] R. LAI, Y. SHI, K. SCHEIBEL, S. FEARS, R. WOODS, A. W. TOGA, AND T. F. CHAN, *Metric-induced optimal embedding for intrinsic 3D shape analysis*, IEEE Conference on Computer Vision and Pattern Recognition (CVPR), (2010).

[33] B. LEVY, *Laplace-beltrami eigenfunctions: Towards an algorithm that understands geometry*, IEEE Interna-

tional Conference on Shape Modeling and Applications, invited talk, (2006).
[34] H. LING AND D. W. JACOBS, *Shape classification using the inner-distance*, IEEE Trans. Pattern Anal. Machine Intell., 29 (2007), pp. 286–299.
[35] L. M. LUI, S. THIRUVENKADAM, Y. WANG, P. THOMPSON, AND T. F. CHAN, *Optimized conformal surface registration with shape-based landmark matching*, SIAM J. Imaging Sciences, 3 (2010), pp. 52–78.
[36] F. LUO, *Geodesic length functions and Teichmüller spaces*, J. Differetial Geometry, 48 (1998).
[37] H. MCKEAN AND I. SINGER, *Curvature and the eigenvalues of the laplacian*, J Differ Geom, 1 (1967), pp. 43–69.
[38] F. MÉMOLI, *On the use of gromov-hausdorff distances for shape comparison*, In Proceedings of Point Based Graphics, Prague, Czech Republic, (2007), pp. 81–90.
[39] ———, *Gromov-hausdorff distances in euclidean spaces.*, Workshop on Non-Rigid Shape Analysis and Deformable Image Alignment (CVPR workshop, NORDIA'08), (2008).
[40] ———, *A spectral notion of Gromov-Wasserstein distances and related methods*, Journal of Applied and Computational Harmonic Analysis, 363–401 (2011).
[41] F. MÉMOLI AND G. SAPIRO, *A theoretical and computational framework for isometry invariant recognition of point cloud data*, Found. Comput. Math., 5 (2005), pp. 313–347.
[42] J. MILNOR, *Eigenvalues of the laplace operator on certain manifolds*, Proc. Nat. Acad. Sci. U.S.A., 51 (1964), p. 542.
[43] ROBERT OSADA, THOMAS FUNKHOUSER, BERNARD CHAZELLE, AND DAVID DOBKIN, *Shape distributions*, ACM Trans. Graph., 21 (2002), pp. 807–832.
[44] M. H. PROTTER, *Can one hear the shape of a drum? revisited*, SIAM Rev, 29 (1987), pp. 185–197.
[45] A. QIU, D. BITOUK, AND M. I. MILLER, *Smooth functional and structural maps on the neocortex via orthonormal bases of the Laplace-Beltrami operator*, IEEE Trans. Med. Imag., 25 (2006), pp. 1296–1306.
[46] M. REUTER, *Hierarchical shape segmentation and registration via topological features of laplace-beltrami eigenfunctions*, International Journal of Computer Vision, doi:10.1007/s11263-009-0278-1 (2009).
[47] M. REUTER, F.E. WOLTER, AND N. PEINECKE, *Laplace-Beltrami spectra as Shape-DNA of surfaces and solids*, Computer-Aided Design, 38 (2006), pp. 342–366.
[48] R. M. RUSTAMOV, *Laplace-beltrami eigenfunctions for deformation invariant shape representation*, Eurographics Symposium on Geometry Processing, (2007).
[49] R. SCHOEN AND S.-T. YAU, *Lectures on Differential Geometry*, International Press, 1994.
[50] Y. SHI, R. LAI, K. KERN, N. SICOTTE, I. DINOV, AND A. W. TOGA, *Harmonic surface mapping with Laplace-Beltrami eigenmaps*, in Proc. MICCAI, 2008.
[51] Y. SHI, R. LAI, S. KRISHNA, N. SICOTTE, I. DINOV, AND A. W. TOGA, *Anisotropic Laplace-Beltrami eigenmaps: Bridging Reeb graphs and skeletons*, in Proc. MMBIA, 2008.
[52] Y. SHI, R. LAI, J. MORRA, I. DINOV, P. THOMPSON, AND A. W. TOGA, *Robust surface reconstruction via laplace-beltrami eigen-projection and boundary deformation*, IEEE Trans. Medical Imaging, 29 (2010), pp. 2009–2022.
[53] Y. SHI, P. M. THOMPSON, I. DINOV, S. OSHER, AND A. W. TOGA, *Direct cortical mapping via solving partial differential equations on implicit surfaces*, Medical Image Analysis, 11 (2007), pp. 207–223.
[54] Y. SHI, Z. TU, A. REISS, R. DUTTON, A. D. LEE, A. GALABURDA, I. DINOV, P. M. THOMPSON, AND A. W. TOGA, *Joint sulcal detection on cortical surfaces with graphical models and boosted priors*, IEEE Trans. Med. Imag., 28 (2009), pp. 361–373.
[55] J. SUN, M. OVSJANIKOV, AND L. GUIBAS, *A concise and provably informative multi-scale signature baded on heat diffusion*, Eurographics Symposium on Geometry Processing, (2009).
[56] T. SUNADA, *Riemannian coverings and isospectral manifolds*, Ann. of Math., 121 (1985), pp. 169–186.
[57] J. W. TANGELDER AND R. C. VELTKAMP, *A survey of content based 3d shape retrieval methods*, Multimedia Tools and Applications, 39 (2008), pp. 441–471.
[58] P. M. THOMPSON, K. M. HAYASHI, G. I. DE ZUBICARAY, A. L. JANKE, S. E. ROSE, J. SEMPLE, D. H. HERMAN, M. S. HONG, S. S. DITTMER, D. M. DODDRELL, AND A. W. TOGA, *Dynamics of gray matter loss in Alzheimer disease*, J. Neurosci., 23 (2003), pp. 994–1005.
[59] K. UHLENBECK, *Generic properties of eigenfunctions*, Amer. J. of Math., 98 (1976), pp. 1059–1078.
[60] B. VALLET AND B. LEVYVY, *Spectral geometry processing with manifold harmonics*, Computer Graphics Forum (Proceedings Eurographics), (2008).
[61] S. WANG, Y. WANG, M. JIN, X. GU, AND D. SAMARAS, *Conformal geometry and its applications on 3d shape matching, recognition and stithching*, IEEE Trans. PAMI, 29 (2007), pp. 1209–1220.
[62] R. P. WOODS, S. C. FEARS, M. J. JORGENSEN, L. A. FAIRBANKS, A. W. TOGA, AND N. B. FREIMER, *A web-based atlas of the vervet monkey, chlorocebus aethiops*, NeuroImage, 54 (2011), pp. 1872–1880.
[63] W. ZENG, Y. ZENG, Y. WANG, X. YIN, X. GU, AND D. SAMARAS, *3d non-rigid surface matching and registration based on holomorphic differerntials*, ECCV, (2008).
[64] Y. ZENG, C. WANG, Y. WANG, X. GU, D. SAMARAS, AND N. PARAGIOS, *Dense non-rigid surface regis-*

tration using high-order graph matching, CVPR, (2010).
[65] D. ZHANG AND M. HEBERT, *Hamonic maps and their applications in surface matching*, CVPR, (1999).